*Journal of Statistical Physics, Vol. 63, Nos. 3/4, 1991*

# Dynamical and Spatial Aspects of Sandpile Cellular Automata

**Kim Christensen,[1] Hans C. Fogedby,[1] and Henrik Jeldtoft Jensen[1]**

*Received October 26, 1990*

The Bak, Tang, and Wiesenfeld cellular automaton is simulated in 1, 2, 3, 4, and 5 dimensions. We define a (new) set of scaling exponents by introducing the concept of conditional expectation values. Scaling relations are derived and checked numerically and the critical dimension is discussed. We address the problem of the mass dimension of the avalanches and find that the avalanches are noncompact for dimensions larger than 2. The scaling of the power spectrum derives from the assumption that the instantaneous dissipation rate of the individual avalanches obeys a simple scaling relation. Primarily, the results of our work show that the flow of sand down the slope does not have a $1/f$ power spectrum in any dimension, although the model does show clear critical behavior with scaling exponents depending on the dimension. The power spectrum behaves as $1/f^2$ in all the dimensions considered.

**KEY WORDS:** Self-organized critical behavior; sandpiles; scaling relations; power spectra.

## 1. INTRODUCTION

It has been a long-standing puzzle why $1/f$ power spectra are seen in a variety of physical systems.[1] Also, the occurrence of spatial fractal structures has been realized as an empirical fact in many different systems,[2] although a proper understanding of the physical origin is still lacking. In a recent paper by Bak, Tang, and Wiesenfeld (BTW),[3] it was suggested that the frequent occurrence of $1/f$ noise and fractal structures is the generic temporal and spatial characteristic of a dynamical critical state into which dynamical systems with many spatial degrees of freedom evolve

[1] Institute of Physics, University of Aarhus, DK-8000 Aarhus C, Denmark.
[2] NORDITA, Blegdamsvej 17, DK-2100 Copenhagen Ø, Denmark.



0022-4715/91/0500-0653$06.50/0 

naturally. Unlike phase transitions in an equilibrium system, a driven dissipative dynamical many-body system reaches the critical state without the need to fine tune the system parameters, i.e., the critical state studied by BTW is an attractor of the dynamics. Therefore, the critical state is usually described as being self-organized, and the phenomena of self-organized criticality (SOC) may very well provide a connection between the occurrence of $1/f$ noise and fractal structures, as well as being the physical origin of these two intriguing phenomena.

This fascinating idea has initiated much work on the critical behavior of driven dissipative dynamical many-body systems: (a) general aspects of SOC,[4–23] (b) scaling and critical exponents,[24–33] (c) SOC applied to earthquakes,[34–39] and (d) experimental findings.[40–45]

In order to visualize the basic idea of self-organized criticality, imagine a sunny day at the beach and a square table. Having noting better to do, we begin sprinkling grains of sand on the table, one grain at a time. We drop the grain on a randomly chosen place on the table and repeat the act when all motion has terminated. In the beginning the grains just fall down on the table in no particular patern. But, subsequently, while continuing to add new grains of sand, we notice the formation of small local avalanches. It is the mechanism of the local avalanches to decrease the local slopes whenever they become to steep. Perturbing the system, the small sandpiles, provoked by avalanches, create still greater sandpiles and, eventually, we end up with only one big sandpile. At some point (the transient time) this pile ceases to grow. The (global) average slope has reached a steady state corresponding to the angle of repose which the sandpile cannot exceed no matter how long we carry on adding sand: The pile has reached a statistically stationary state, and additional grains of sand will ultimately fall off the pile.

Likewise, we notice the unpredictability concerning the size of the avalanches, although they are clearly necessary in order to relax the sandpile. Even though the sandpile is driven to the stationary state, we still observe a variation of the local slopes (state variables) of the sandpile. But the local slopes of the pile cannot exceed a specific critical value without a grain of sand tumbling down. When the local slope equals the critical value, it is called *a minimally stable site.* An avalanche is triggered the moment we add a grain of sand which causes the local slope to exceed the critical value. This will inevitably happen if our grain of sand provokes a positive change of a minimally stable site. Roughly speaking, an avalanche sweeps the minimally stable sites that are spatially connected. The variation of the local slopes makes it impossible to predict what is going to happen when we add a new particle of sand. Either it triggers a global avalanche, or the perturbation only results in small local rearrangements, and, occasionally,

the additional grain of sand just rests where it falls; no avalanche is produced.

In order to examine the phenomenon of self-organized criticality, BTW[3] introduced a cellular automaton. A cellular automaton involves discrete space coordinates and discrete time steps. Furthermore, the physical quantities that are connected with the lattice sites only take on a finite set of discrete values. The state of the cellular automaton is completely specified by the values of the physical variables on each site. The dynamical rules for the physical variables determine the evolution of the model. The dynamical rules in the BTW model, at least intuitively, resemble the dynamics of a sandpile: A signal is transmitted from a local site to its nearest neighbors when a dynamical integer variable exceeds a threshold value.

By simulating this model, BTW showed that the system does indeed drive itself into a statistically stationary state, characterized by distributions of avalanche lifetimes and avalanche sizes which exhibit power law behavior. Hence, the system evolves into a stationary state without any characteristic time or length scales and is in this sense critical. The generic universality of the model stems from the very simple nonlinear diffusion equation governing the dynamics of the system.

We intend to discuss in detail the different versions of the BTW sandpile cellular automaton model. In Section 2, we introduce the model and describe the different excitation mechanisms and boundary conditions considered in our simulations. In Section 3, we define scaling exponents for both probability densities and conditional expectation value. The various scaling exponents are connected by means of scaling relations. Section 4 includes a derivation of the scaling properties for the power spectrum from a scaling annsatz of the dissipation rate of the individual avalanches. In Section 5 we summarize the results of computer simulations in dimensions 1–5, and, finally, the scaling relations are discussed.

Initially, the idea was to explain the mechanism behind $1/f$ noise and fractal structures, but the BTW model does not contain a $1/f$ power spectrum for the flow of sand down the slope. The model seems to contain a $1/f^2$ power spectrum[18] irrespective of the dimension, at least in the case of dimensions 1–5. It is not yet settled, to what extent the spatial properties are characterized by fractals. We find that the avalanches are noncompact in dimensions higher than 2. It has been suggested[26,29] that the critical dimension of (one version of) the model is 4. Some of the measured exponents seem to change from 4 to 5 dimensions, indicating a critical dimension larger than 4.

## 2. DEFINITION OF THE SANDPILE CELLULAR AUTOMATA

The model is a cellular automaton defined on a $d$-dimensional cubic lattice of linear size $N$: For a given set of canonical basis vectors $\{\mathbf{e}_i\}$, $i = 1,..., d$, wed define a $d$-dimensional cubic lattice $\mathscr{L}^d$ of linear size $N$ as the collection of points

$$\mathbf{r} = \sum_{i=1}^{d} r_i \mathbf{e}_i \tag{1}$$

where the $i$th coordinate $r_i$ is an integer restricted to the interval between 0 and $N$. To each lattice site $\mathbf{r} \in \mathscr{L}^d$ we assign an integer $z(\mathbf{r})$ which is to represent a discrete version of an appropriate dynamical variable on site $\mathbf{r}$ of a spatially extended dynamical system.

A point in phase space of the $d$-dimensional dynamical system is completely specified by the total set of dynamical variables $\{z(\mathbf{r})\}$, $\mathbf{r} \in \mathscr{L}^d$, i.e., a trajectory in phase space corresponds to a particular evolution of the dynamical system.

The dynamical rules (the perturbation mechanism and the relaxation rules) of the $d$-dimensional model have been motivated by the following heuristic considerations on the two-dimensional version of the model[10]: We think of sand particles as positioned on the bonds between the lattice sites $\mathbf{r} \in \mathscr{L}^2$. We define a scalar $z(i, j)$ as the average local slope on site $(i, j)$ by $z(i, j) = h_1 + h_2 - h_3 - h_4$, where $h_k$ denotes the height of the column of sand on the $k$th bond at site $(i, j)$ (see Fig. 1).

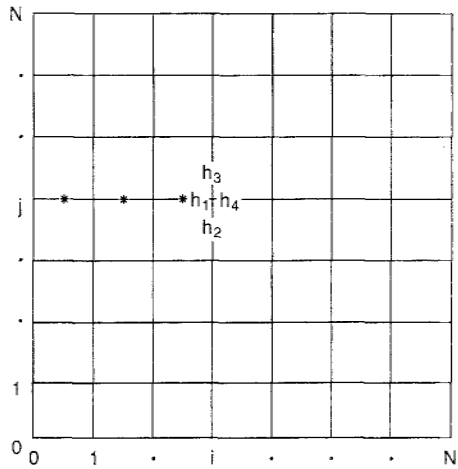


Fig. 1. Two-dimensional lattice of linear size $N$. The values of $h_k$ represent the heights of the columns of sand on the bonds connecting site $(i, j)$ to its neighbors. The meaning of the asterisks is explained in the text. Note that there is no one-to-one correspondence between the heights and the slopes for dimensions above one.

We examine two different perturbation mechanisms. First, bearing in mind the heuristic sandpile picture, we add two grains of sand locally on bond 1 and 2 at site $\mathbf{r} \in \mathscr{L}^2$. With regard to the local slope, this results in a *conservative perturbation mechanism* which, when generalized to a $d$-dimensional system, takes the form

$$\begin{aligned} z(\mathbf{r}) &\to z(\mathbf{r}) + d \\ z(\mathbf{r} - \mathbf{e}_i) &\to z(\mathbf{r} - \mathbf{e}_i) - 1 \qquad \text{for} \quad i = 1,..., d \end{aligned} \tag{2}$$

Second, we consider the *nonconservative perturbation mechanism*

$$z(\mathbf{r}) \to z(\mathbf{r}) + 1 \tag{3}$$

which, in the sandpile picture, corresponds to a nonlocal change of the height of the columns, for instance, by adding one grain of sand to all the columns marked by an asterisk in Fig. 1.

Whenever the local slope exceeds a certain *critical slope* $z_c$ sand tumbles from the higher to the lower columns. This causes two grains of sand to tumble from the columns on bond 1 and 2 to the columns on bond 3 and 4. The corresponding changes in the $z$ values will be given according to the following *relaxation* algorithm:

$$\begin{aligned} \text{If } z(\mathbf{r}) > z_c, \text{ then} \qquad & z(\mathbf{r}) \to z(\mathbf{r}) - 2d \\ & z(\mathbf{r} \pm \mathbf{e}_i) \to z(\mathbf{r} \pm \mathbf{e}_i) + 1 \qquad \text{for} \quad i = 1,..., d \end{aligned} \tag{4}$$

If several sites $\mathbf{r} \in \mathscr{L}^d$ are unstable, $z(\mathbf{r}) > z_c$, the relaxations will take place simultaneously.

Since the lattice $\mathscr{L}^d$ is finite, we have to define the boundary conditions. We examine two different types of boundary conditions. First, we allow sand to leave the system over the two edges by imposing *open boundary conditions*, i.e., the algorithm in Eq. (4) is changed to

$$\begin{aligned} z(\mathbf{r}) &\to z(\mathbf{r}) - 2d + (\text{number of } i \text{ with } r_i = N) \\ z(\mathbf{r} + \mathbf{e}_i) &\to z(\mathbf{r} + \mathbf{e}_i) + 1 \qquad \text{if} \quad r_i \neq N \\ z(\mathbf{r} - \mathbf{e}_i) &\to z(\mathbf{r} - \mathbf{e}_i) + 1 \qquad \text{for} \quad i = 1,..., d \end{aligned}$$

while

$$z(\mathbf{r}) = 0 \qquad \text{if there exists} \quad r_j = 0 \tag{5}$$

Second, we prevent sand from leaving the system by imposing *closed boundary conditions*, i.e.,

$$z(\mathbf{r}) = 0 \qquad \text{if there exists} \quad r_j = 0 \quad \text{or} \quad r_j = N \tag{6}$$

If we have chosen a perturbation mechanism and a set of boundary conditions, then the algorithm of the temporal evolution of the sandpile cellular automaton follows:

Algorithm 1.

1. Specify an initial configuration $\{z(\mathbf{r})\}$.
2. If any $z(\mathbf{r}) > z_c$, then relax the configuration simultaneously by use of Eq. (4), taking into account the chosen boundary conditions until $z(\mathbf{r}) \leqslant z_c$ for all sites $\mathbf{r}$.
3. Choose a position $\mathbf{r}$ at random. Perturb the system according to the specified perturbation mechanism. Return to step 2.

We define a *unit time-step* as one update of the whole latice. Let $\langle z \rangle(\tau)$ denote the $z$ value averaged over sites $\mathbf{r} \in \mathscr{L}^d$. After a transient period, during which $\langle z \rangle(\tau)$ increases, a *stationary state* is reached: $\langle z \rangle(\tau)$ fluctuates around an average value

$$\overline{\langle z \rangle} = \lim_{T \to \infty} \frac{1}{T} \int_0^T \langle z \rangle(\tau)\, d\tau \tag{7}$$

In Fig. 2 we show examples of the time evolution of the average $z$ values for the two different perturbation mechanisms in a two-dimensional system with open boundaries. Both simulations have been started from an initial configuration with all the $z$ values set equal to zero. We notice that the nonconservative perturbation mechanism produces a stationary critical

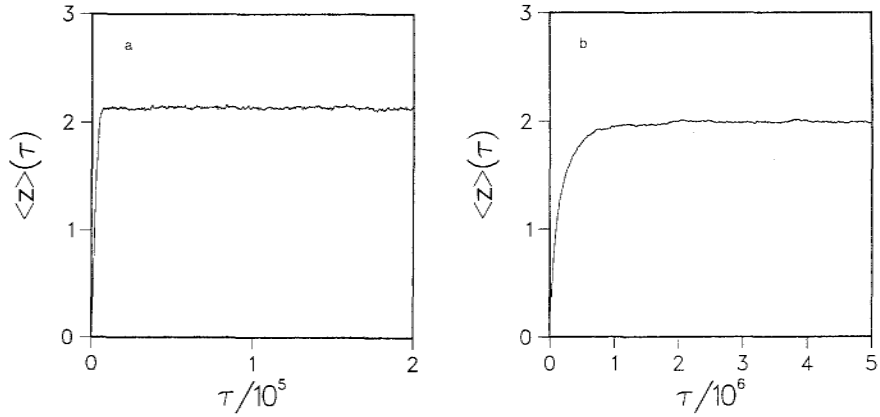


Fig. 2. The spatial averaged slope $\langle z \rangle(\tau)$ as a function of time for systems with open boundary conditions. (a) System driven by the nonconservative perturbation mechanism; see Eq. (3). (b) System driven by the conservative perturbation mechanism; see Eq. (2).

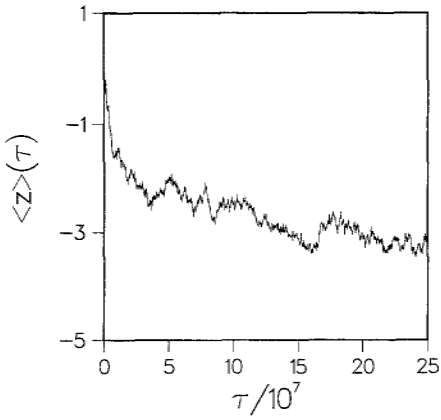


Fig. 3. The spatial averaged slope $\langle z \rangle(\tau)$ as function of time for a system with closed boundary conditions driven by the conservative perturbation mechanism; see Eq. (2).

state much faster than the conservative perturbation mechanism. The time variation of the $z$ values has its origin in: (a) the nonconservative changes of the $z$ values on the closed boundaries and (b) the nonconservative perturbation mechanism. In a situation with closed boundary conditions and conservative perturbation mechanism the system never reaches a stationary state (see Fig. 3). This is an artifact of using $z > z_c$ rather than the more physical condition $|z| > z_c$ as the threshold criterion. In a situation where only $z > z_c$ trigers off a relaxation, the average slope decreases without limit due to the closed boundary conditions. On the other hand, the nonconservative perturbation mechanism combined with closed boundary conditions produces a stationary state. In such a case $z(\mathbf{r})$ never becomes negative when $z_c = 2d - 1$ is used. The results are independent of the specific value of $z_c$.

## 3. SCALING EXPONENTS

For the purpose of giving a precise definition of the scaling exponents we must provide a concise definition of the statistical properties of the sandpile automata in terms of an ensemble. First we concentrate on a member of the ensemble labeled by $i$. Introduce an indicator function of unstable sites at time $\tau$ on the lattice corresponding to the $i$th member

$$f_i(\mathbf{r}, \tau) = \begin{cases} 1 & \text{if } z(\mathbf{r}) > z_c \\ 0 & \text{otherwise} \end{cases} \tag{8}$$

We define the *instantaneous dissipation rate* of an avalanche $\alpha$ in the $i$th member of the ensemble by

$$f_{\alpha_i}(\tau) = \sum_{\mathbf{r}} f_i(\mathbf{r}, \tau) \tag{9}$$

where the summation is over all lattice sites $\mathbf{r}$ in system number $i$. In other words, we assign to each avalanche (outcome) a function of time, whose value at time $\tau$ equals the total number of relaxations at that instant. The family of all such functions $\{f_{\alpha_i}(\tau)\}$ defines a *stochastic process* $X(\tau)$ (see Fig. 4).

Next, we introduce a probability density on the set $\{f_{\alpha_i}(\tau)\}$. Given a particular dissipation rate $f_\alpha(\tau)$, we define an indicator function by

$$I[f_{\alpha_i}(\tau)] = \begin{cases} 1 & \text{if } f_{\alpha_i}(\tau) = f_\alpha(\tau) \text{ for all } \tau \\ 0 & \text{otherwise} \end{cases} \tag{10}$$

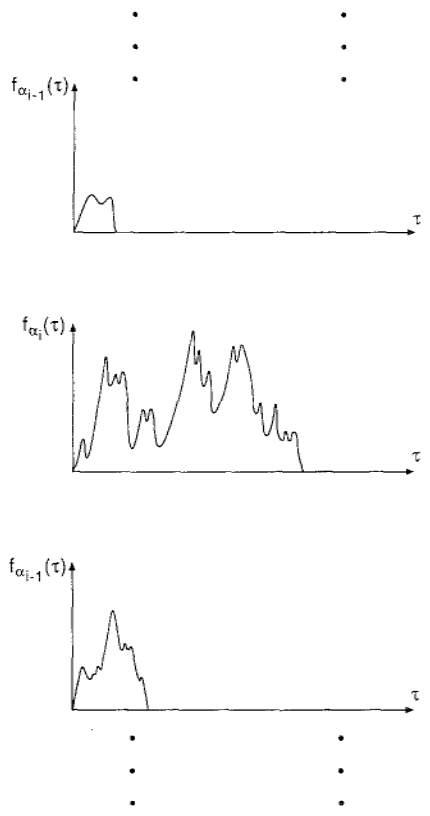


Fig. 4. Three realizations $f_{\alpha_i}(\tau)$ of the stochastic process $X(\tau)$.

The considered ensemble defines the probability for producing an avalanche with a temporal characterization $f_\alpha(\tau)$ by

$$P[X(\tau)=f_\alpha(\tau)]=\lim_{n\to\infty}\frac{\sum_{i=1}^{n} I[f_{\alpha_i}(\tau)]}{n} \tag{11}$$

The *total dissipation* (or size) of an avalanche of type $f_\alpha(\tau)$ is defined as

$$s=\int_0^\infty f_\alpha(\tau)\,d\tau \tag{12}$$

and the *lifetime* of the avalanche started at time $\tau=0$ is

$$t=\max\{\tau\,|\,f_\alpha(\tau)>0\} \tag{13}$$

while we define the *spatial linear size* of the avalanche as the maximum distance to a perimeter point from the initial perturbation lattice point $\mathbf{r}_0$:

$$l=\max\{d\,|\,d=\mathrm{dist}(\mathbf{r},\mathbf{r}_0)\text{: }\mathbf{r}\text{ is within the avalanche}\} \tag{14}$$

The probability densities of the corresponding stochastic variables $S$, $T$, and $L$ are given by

$$\begin{aligned}
P(S=s)&=\sum_\alpha P\left[X(t)=f_\alpha(t)\,\middle|\int_0^\infty f_\alpha(\tau)\,d\tau=s\right]\\
P(T=t)&=\sum_\alpha P[X(t)=f_\alpha(t)\,|\max\{\tau\,|\,f_\alpha(\tau)>0\}=t]\\
P(L=l)&=\sum_\alpha P[X(t)=f_\alpha(t)\,|\\
&\qquad \max\{d\,|\,d=\mathrm{dist}(\mathbf{r},\mathbf{r}_0)\text{: }\mathbf{r}\text{ is within the avalanche}\}=l]
\end{aligned} \tag{15}$$

i.e., the summations are restricted to avalanches of size $s$, lifetime $t$, and linear size $l$, respectively.

Finally, we introduce[3] the *scaling exponents* $\tau$, $\alpha$, and $\lambda$ by means of

$$\begin{aligned}
P(S=s)&\sim s^{1-\tau}\\
P(T=t)&\sim t^{1-\alpha}\\
P(L=l)&\sim l^{1-\lambda}
\end{aligned} \tag{16}$$

[3] The notation for the scaling exponents is that used in the literature, and should be distinguished from the time variable $\tau$ and the avalanche index $\alpha$.

and the following set of *conditional expectation values* with corresponding exponents:

$$\begin{aligned} E[S \mid T=t] &\sim t^{\gamma_1} \\ E[T \mid S=s] &\sim s^{1/\gamma_1} \\ E[S \mid L=l] &\sim l^{\gamma_2} \\ E[L \mid S=s] &\sim s^{1/\gamma_2} \\ E[T \mid L=l] &\sim l^{\gamma_3} \\ E[L \mid T=t] &\sim t^{1/\gamma_3} \end{aligned} \tag{17}$$

where, for example,

$$E[S \mid T=t] = \sum_s sP(S=s \mid T=t) \tag{18}$$

The reciprocal relationship between the exponents shown in Eq. (17) is a necessary condition if we assume the existence of transformations that relate the stochastic variable $S$ with $T$, $S$ with $L$, and $T$ with $L$ (see Fig. 5). In a strictly mathematical sense such transformations cannot exist since, as an example, there will always be more than one possible avalanche size $s$ for a given lifetime $t$. However, we find that the reciprocal relationships are fulfilled quite accurately (see Section 5), which indicates that the conditional densities, e.g., $P(S=s \mid T=t)$, have a narrow support around their average value.

In order to obtain scaling relations between the exponents, we bear in mind the general identity involving three stochastic variables $X$, $Y$, and $Z$:

$$\int E[X \mid Y=y]\, P(Y=y)\, dy = \int E[X \mid Z=z]\, P(Z=z)\, dz \tag{19}$$

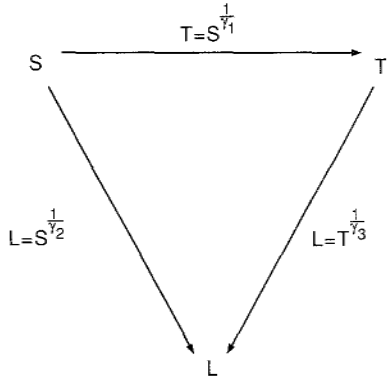


Fig. 5. Transformation relation connecting the stochastic variables $S$, $T$, and $L$.

following from the fact that both integrals produce the expectation value of $X$, $E(X)$. For $\{X, Y, Z\} = \{S, T, L\}$ we substitute Eqs. (16) and (17) into Eq. (19) and obtain

$$\int dt\, t^{\gamma_1} t^{1-\alpha} = \int dl\, l^{\gamma_2} l^{1-\lambda} \tag{20}$$

in the case of $X = S$, $Y = T$, and $Z = L$. We assume a transformation consistent with the scaling ansatz in Eq. (17)

$$L = T^{1/\gamma_3} \tag{21}$$

This leads to

$$\alpha = 2 + \gamma_1 + \frac{\lambda - \gamma_2 - 2}{\gamma_3} \tag{22}$$

In the case of $X = T$, $Y = S$, and $Z = L$, we obtain in a similar way

$$\tau = 2 + \frac{1}{\gamma_1} + \frac{\lambda - \gamma_3 - 2}{\gamma_2} \tag{23}$$

and, finally, $X = L$, $Y = S$, and $Z = T$ produce the identity

$$\tau = 2 + \frac{1}{\gamma_2} + \frac{\alpha\gamma_3 - 2\gamma_3 - 1}{\gamma_1\gamma_3} \tag{24}$$

Substituting Eq. (22) into Eq. (24) and comparing with Eq. (23), we obtain

$$\gamma_2 = \gamma_1\gamma_3 \tag{25}$$

in accordance with the assumed relationships between $S$, $T$, and $L$ as outlined in Fig. 5. Introducing Eq. (25) in Eqs. (22) and (23), we obtain the simple expressions

$$\begin{aligned} \alpha &= 2 + \frac{\lambda - 2}{\gamma_3} \\ \tau &= 2 + \frac{\lambda - 2}{\gamma_2} \end{aligned} \tag{26}$$

## 4. POWER SPECTRUM

In this section, we analyze the response of the sandpile automaton (the flow of sand down the slope of the sandpile) due to white-noise perturbations (adding sand randomly in space and time) in the frequency domain.

We consider a system in the stationary state and perturb it by adding sand, on randomly chosen lattice sites, with a constant probability $\nu$ per time. For a sufficiently large system we can neglect the interference between different avalanches. Hence, the total dissipation rate $j(\tau)$ at a given time $\tau$ equals the linear superposition of the individual dissipation rates produced by the individual avalanches operating at time $\tau$ (see Fig. 6). To produce a mathematical expression for the total dissipation rate, we introduce a family of discrete (indicator) functions $\{p^\alpha(\tau)\}_\alpha$. With a fixed $\alpha$ the function $p^\alpha(\tau)$ is equal to unity if an avalanche of type $\alpha$ has been triggered off in the time segment $\tau, \tau + d\tau$, zero otherwise. If we divide the time axis into intervals of length $\delta$, then

$$j(\tau) = \sum_\alpha \sum_{n=-\infty}^{\tau/\delta} f_\alpha(\tau - n\delta)\, p^\alpha(n\delta)$$

$$= \sum_\alpha \sum_{n=-\infty}^{\infty} f_\alpha(\tau - n\delta)\, p^\alpha(n\delta) \tag{27}$$

where the second equality in Eq. (27) is a consequence of using the convention $f_\alpha(\tau) = 0$ when $\tau < 0$. A specific time evolution $j(\tau)$ of a given system is completely characterized by the map (see Fig. 7)

$$\alpha, n \mapsto p^\alpha(n\delta) \tag{28}$$

We introduce an ensemble of critical systems where each ensemble member is perturbed by adding sand (on randomly chosen sites) with a constant probability rate $\nu$. Consequently (with fixed $\alpha$) this leads to a transformation of the function $p^\alpha(n\delta)$ into a stochastic process $P^\alpha(n\delta)$. Replacing $p^\alpha(n\delta)$ with $P^\alpha(n\delta)$ in Eq. (27), we turn $j(\tau)$ into a stochastic

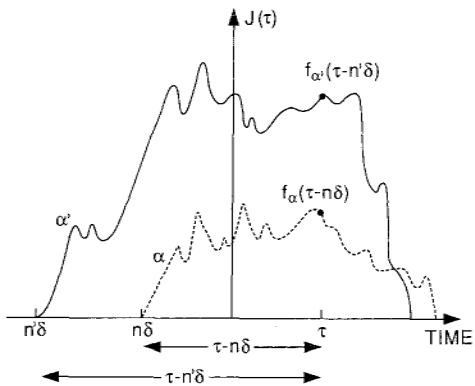


Fig. 6. Linear superposition of avalanches.

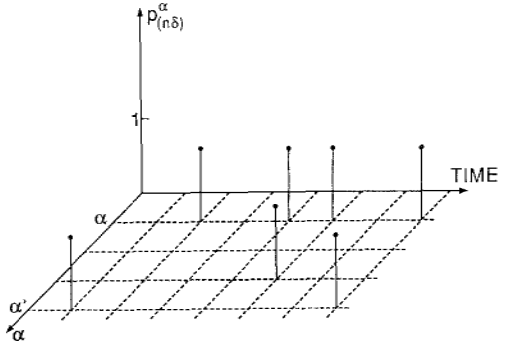


Fig. 7. Schematic representation of the map in Eq. (28).

process $J(r)$. For each realization $j(\tau)$ of the stochastic process $J(\tau)$ we perform the Fourier transform[47,48]

$$\hat{j}(\omega) = \int_{-\infty}^{\infty} j(\tau) e^{-i\omega\tau}\, d\tau \tag{29}$$

and the corresponding power spectrum is given by

$$S_j(\omega) = |\hat{j}(\omega)|^2 \tag{30}$$

$S_j(\omega)$ is a strongly fluctuating function of $\omega$, since we are dealing with a random variable with respect to the random process $J(\tau)$. Performing the ensemble average

$$S_J(\omega) = E[S_j(\omega)] \tag{31}$$

we obtain a smooth function of the frequency $f = \omega/2\pi$.

The method outlined above, used to establish the power spectrum, is suitable when we want to measure the power spectrum directly. However, for analytical analysis, we find that the concept of an autocorrelation function is more convenient. It turns out that the power spectrum of the stochastic process $J(\tau)$ can be expressed in terms of a weighted average of the power spectra of individual $f_\alpha(\tau)$ signals (see Appendix A):

$$S_J(\omega) = \nu \sum_{\alpha} P(\alpha)\, |\hat{f}_\alpha(\omega)|^2 \tag{32}$$

$P(\alpha)$ denotes the probability for an avalanche of type $\alpha$ to occur. From this expression we derived the scaling properties of $S_J(\omega)$. First, we assume that

it is possible to characterize the individual avalanche signals by the size and lifetime, i.e., $\alpha = (s, t)$. Furthermore, the identity

$$\int_0^t f_{s,t}(\tau)\, d\tau = s = \int_0^t \frac{s}{t} f_{1,1}\left(\frac{\tau}{t}\right) d\tau$$

suggests the scaling relation (see Fig. 8)

$$f_{s,t}(\tau) = \frac{s}{t} f_{1,1}\left(\frac{\tau}{t}\right) \tag{33}$$

Considering the Fourier transform, the scaling relation in the time domain is transformed into a scaling relation in the frequency domain:

$$\hat{f}_{s,t}(\omega) = s\hat{f}_{1,1}(\omega t) \tag{34}$$

Substituting Eq. (34) into Eq. (32), we obtain the fundamental equation for the analysis of the dynamical aspects of the sandpile

$$S_J(\omega) = v \sum_s \sum_t |\hat{f}_{1,1}(\omega t)|^2 s^2 P(S = s,\ T = t) \tag{35}$$

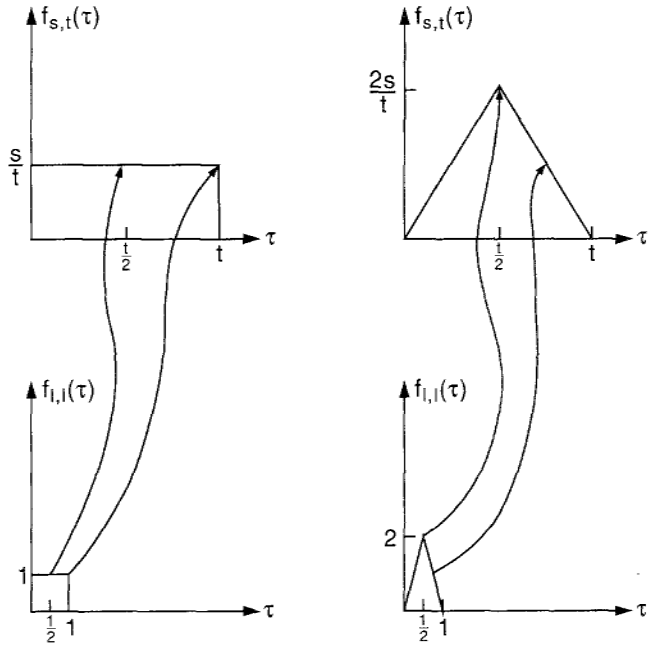


Fig. 8. Two examples of elementary avalanche signals scaled according to Eq. (33).

Three different frequency regions have to be considered: A low-, an intermediate-, and a high-frequency region. For $\omega \to 0$ the power spectrum becomes white, since the linear superimposed signal $J(\tau)$ cannot contain correlations for times longer than the longest possible lifetime $t_{\max}$ of an avalanche, i.e., $S(\omega) \to \text{const}$ when $\omega < 1/t_{\max}$. In the high-frequency region, $S_J(\omega) \sim \omega^{\alpha_\infty}$. The value of the exponent $\alpha_\infty$ depends on the specific form of $f_{1,1}(\tau)$. The behavior of $S_J(\omega)$ for intermediate frequencies is determined by $P(S=s,\ T=t)$. We introduce a weighted lifetime distribution $A(t)$ by

$$A(t) = \sum_s s^2 P(S=s,\ T=t) = E[S^2 \mid T=t]\ P(T=t) \tag{36}$$

Assuming that $A(t)$ exhibits a scaling behavior in an interval $0 < t_1 \leqslant t \leqslant t_2 < \infty$,

$$A(t) \sim t^{\mu} \tag{37}$$

and is negligible outside, we have

$$\begin{aligned} S_J(\omega) &\approx v \sum_{t \in [t_1, t_2]} A(t) |\hat{f}_{1,1}(\omega t)|^2 \\ &\approx v\omega^{-\mu-1} \left\{ \int_{\omega t_1}^{1} t^{\mu} |\hat{f}_{1,1}(t)|^2\, dt + \int_{1}^{\omega t_2} t^{\mu} |\hat{f}_{1,1}(t)|^2\, dt \right\} \end{aligned} \tag{38}$$

An analysis of the scaling behavior of the two different terms in this equation is given in Appendix B, and leads to the following result:

$$S_J(\omega) = \begin{cases} 1, & 0 < -\mu - 1 \\ \omega^{-\mu-1}, & \alpha_\infty < -\mu - 1 < 0 \\ \omega^{\alpha_\infty}, & -\mu - 1 < \alpha_\infty \end{cases} \tag{39}$$

For $f_{1,1}(\tau)$ equal to a square box function (see Fig. 8), $\alpha_\infty = -2$, whereas, in the case of a triangular shape of $f_{1,1}(\tau)$, the exponent $\alpha_\infty = -4$. In Appendix B we prove that $\alpha_\infty \leqslant -2$. Thus, the only way to obtain a $1/f$ power spectrum is by having a weighted lifetime distribution with an exponent $\mu = 0$, irrespective of the specific form of the superposed signals!

From Eq. (36) we can derive a scaling relation for the exponent $\mu$ by use of the assumed transformation $S = T^{\gamma_1}$. From Eqs. (36), (25), and (26) we obtain

$$\mu = (4 - \tau)\gamma_1 - 1 \tag{40}$$

## 5. SIMULATION RESULTS

### 5.1. Scaling Exponents

In order to measure the scaling exponents defined in Eqs. (16) and (17) we have made simulations on systems of linear size $N=40$ in two dimensions, $N=20$ in three and four dimensions, and $N=15$ in five dimensions. The simulations are done as follows. Starting from an empty system, $z(\mathbf{r})=0$ for all $\mathbf{r}$, we perform the time evolution procedure described in Algorithm 1 until the stationary state is reached. We measure the joint probability density $P(S=s,\ T=t,\ L=l)$ by consecutively perturbing the system and probe the response until we have obtained sufficient statistics to construct the probability densities and conditional expectation values from Eqs. (15) and (18). It is worthwhile noticing that we replace the above discussed ensemble average by an average over repeatedly executed probings of the same system. This is permitted since the stationary state is independent of the detailed history of the transient period and, moreover, because the perturbation does not drive the system out of the stationary state. In other words, we assume that the system is ergodic.

A set of generated densities for the nonconservative perturbation algorithm defined in Eq. (3) combined with the closed boundary conditions given by Eq. (6) is shown in Fig. 9. These are the directly measured data, i.e., no coarse graining has been done, the used bin size is equal to one. From these plots we infer the scaling exponents and list them in Table I. Exponents for the nonconservative perturbation mechanism defined in Eq. (3) combined with the open bondary conditions are given in Table II. Finally, Table III contains the results for the conservative perturbation mechanism defined by Eq. (2) combined with the open boundary conditions given in Eq. (5). We believe that the exponents are determined within an uncertainty of about $\pm 0.1$.

The exponent $\tau$ is measured from the slope of the graph in Fig. 9a. The columns labeled by $\gamma_1$, $\gamma_2$, and $\gamma_3$ are measured from the slope of the linear part of the graphs in Figs. 9b, 9d, and 9f, respectively. The numbers in the columns labeled by $1/\gamma_1$, $1/\gamma_2$, and $1/\gamma_3$ are obtained from the slopes of Figs. 9c, 9e, and 9g, respectively. By comparing the measured value of $1/\gamma_i$ (with $i=1$, 2, and 3) to the measured $\gamma_i$, we conclude that the assumption of pairwise reciprocal relationships between the scaling exponents in Eq. (17) is fulfilled within the numerical accuracy.

In order to test the scaling relation $\gamma_2=\gamma_1\gamma_3$ in Eq. (25) obtained from the assumed transformation relationship (see Fig. 5), we list in the column labeled by $\gamma_1\gamma_3$ the product of the measured exponents in columns $\gamma_1$ and $\gamma_3$. Furthermore, we have written the product of the measured exponents in columns $1/\gamma_1$ and $1/\gamma_3$ in the column labeled by $1/\gamma_1\gamma_3$. This number is

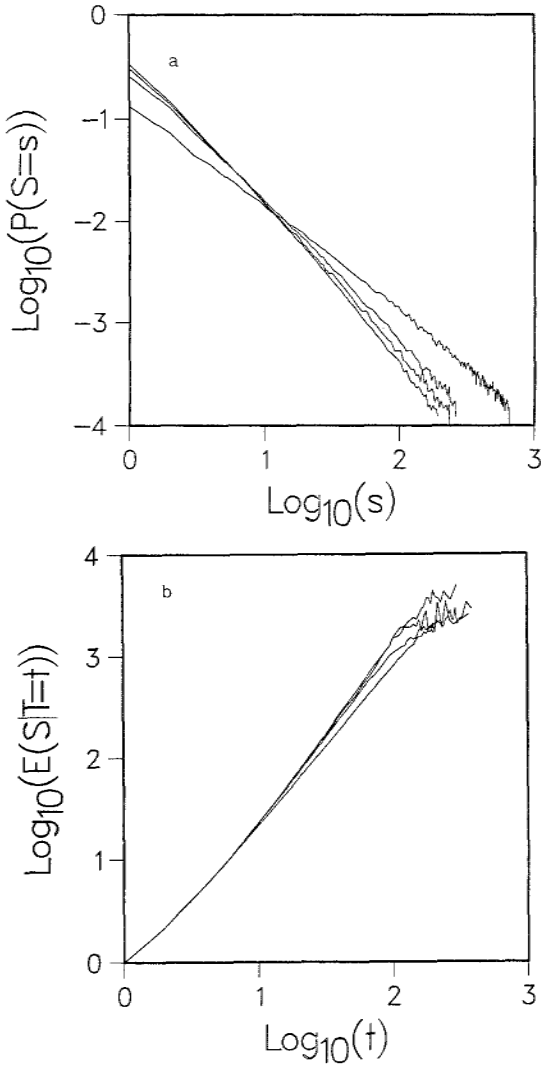


Fig. 9. Simulation results for systems (in two, three, four, and five dimensions) with closed boundary conditions combined with the nonconservative perturbation mechanism. (a) Avalanche sizes. The slope determines the exponent $\tau$. (b) The conditional expectation value of the avalanche sizes for a given lifetime. The slope determines the exponent $\gamma_1$. (c) The conditional expectation value of the avalanche lifetimes for given size. The slope determines the exponent $1/\gamma_1$. (d) The conditional expectation value of the avalanche sizes for given linear size. The slope determines the exponent $\gamma_2$. (e) The conditional expectation value of the linear size of the avalanches for given total size. The slope determines the exponent $1/\gamma_2$. (f) The conditional expectation value of the avalanche lifetime for given linear size. The slope of the straight line determines the exponent $\gamma_3$. (g) The conditional expectation value of linear size for given lifetime. The slope determines the exponent $1/\gamma_3$.

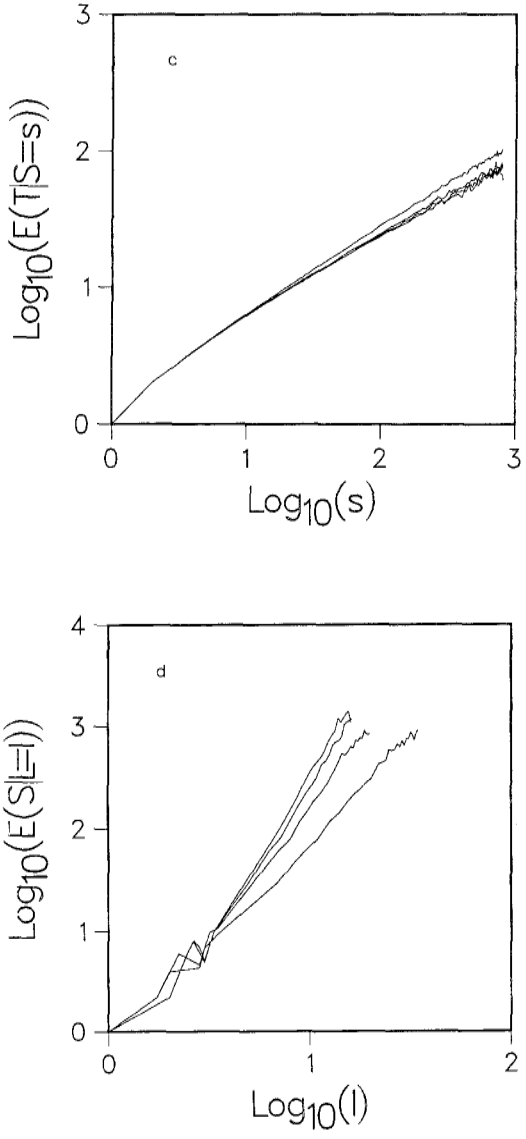


Fig. 9. (*Continued*)

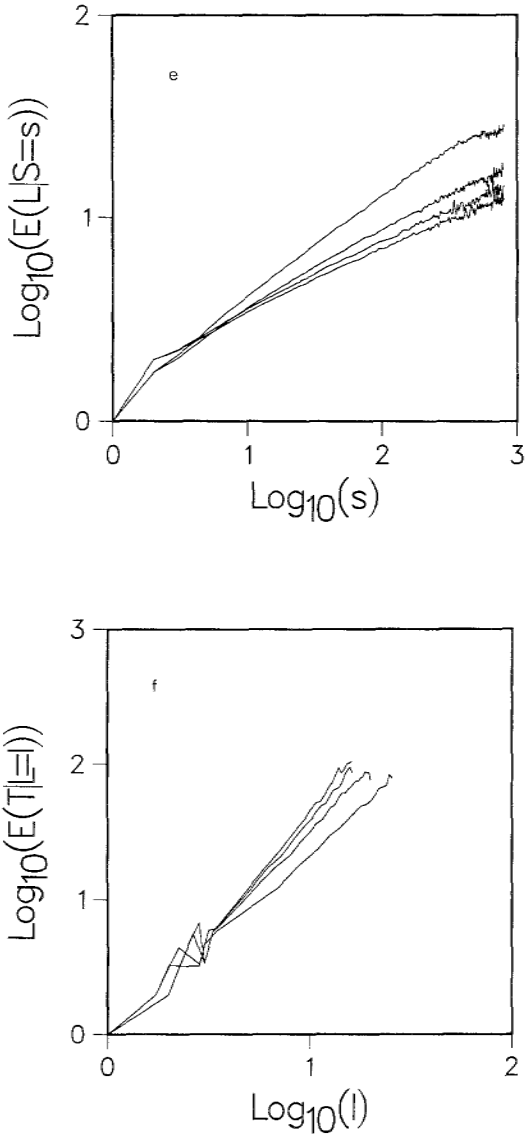


Fig. 9. (*Continued*)

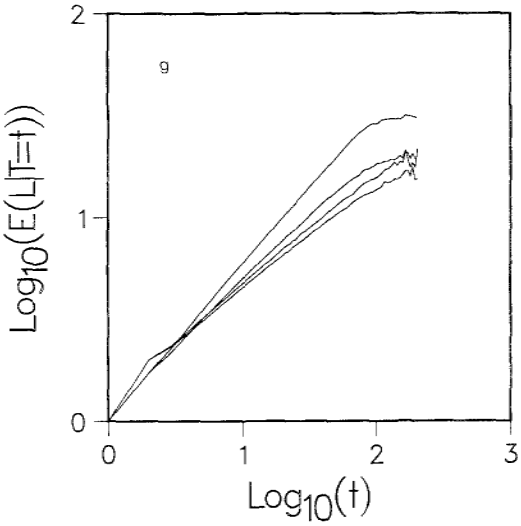


Fig. 9. (*Continued*)

to be compared with the values in column $1/\gamma_2$. We find that this scaling relation is well satisfied.

The exponent $\lambda$ is difficult to obtains from the slope of Fig. 10a. However, in the case of the nonconservative perturbation mechanism and the closed boundary conditions we make a consistency check by use of the scaling relation in Eq. (26). This is done by inserting the measured values (from Table I) in Eq. (26) to obtain a prediction for the value $\lambda$. We obtain $\lambda = 2$ in two dimensions, $\lambda = 3$ for three dimensions, $\lambda = 3.55$ in four dimensions, and $\lambda = 3.94$ in five dimensions. The corresponding slopes $1 - \lambda$ are represented by straight lines in Fig. 10a. We note that these findings are consistent with the numerical measurements. Next, we use the calculated values of $\lambda$ together with the measured value of $\gamma_3$ in Table I to estimate the

**Table I. Simulation Results for Systems (in Two, Three, Four, and Five Dimensions) with Closed Boundary Conditions Combined with the Nonconservative Perturbation Mechanism**

| Dimension | $\tau$ | $\gamma_1$ | $1/\gamma_1$ | $\gamma_2$ | $1/\gamma_2$ | $\gamma_3$ | $1/\gamma_3$ | $\gamma_1\gamma_3$ | $1/\gamma_1\gamma_3$ |
|---|---|---|---|---|---|---|---|---|---|
| 2 | 2.00 | 1.55 | 0.64 | 2.08 | 0.49 | 1.34 | 0.75 | 2.08 | 0.48 |
| 3 | 2.37 | 1.70 | 0.59 | 2.72 | 0.37 | 1.61 | 0.62 | 2.74 | 0.37 |
| 4 | 2.50 | 1.79 | 0.56 | 3.09 | 0.33 | 1.80 | 0.55 | 3.22 | 0.31 |
| 5 | 2.58 | 1.80 | 0.56 | 3.34 | 0.30 | 1.84 | 0.53 | 3.31 | 0.30 |

**Table II. Simulation Results for Systems (in Two, Three, and Four Dimensions) with Open Boundary Conditions Combined with the Nonconservative Perturbation Mechanism**

| Dimension | $\tau$ | $\gamma_1$ | $1/\gamma_1$ | $\gamma_2$ | $1/\gamma_2$ | $\gamma_3$ | $1/\gamma_3$ | $\gamma_1\gamma_3$ | $1/\gamma_1\gamma_3$ |
|---|---|---|---|---|---|---|---|---|---|
| 2 | 2.00 | 1.55 | 0.64 | 2.13 | 0.49 | 1.35 | 0.75 | 2.09 | 0.48 |
| 3 | 2.31 | 1.71 | 0.59 | 2.76 | 0.37 | 1.63 | 0.62 | 2.79 | 0.37 |
| 4 | 2.46 | 1.77 | 0.56 | 3.09 | 0.33 | 1.81 | 0.55 | 3.20 | 0.31 |

exponent $\alpha$ from the scaling relation in Eq. (26). The predicted values yield corresponding slopes for the double logarithmic plots of $P(T=t)$ versus $t$ in Fig. 10b, which are drawn as straight lines in this figure. Also in this case we obtain good agreement between the predicted value for the exponent $\alpha$ and the measured one.

In the case of the nonconservative perturbation mechanism combined with the closed boundary conditions, Zhang[33] has discussed the exponents $\lambda$ and $\gamma_2$ and derived a scaling relation to determine the exponent $\tau$. He used a mean-field-type argument to conclude that the exponent $\lambda$ in Eq. (16) for the density of the spatial linear size equals the Euclidean dimension: $\lambda = d$. As mentioned above, we find $\lambda = d$ except for $d > 3$. Zhang assumes that the avalanches are compact, i.e., the the exponent $\gamma_2$ in Eq. (17) describing the connection between the linear extension of an avalanche and the total size is equal to the Euclidean dimension: $\gamma_2 = d$. As is seen in Table I, our simulations do not appear to be consistent with the equality $\gamma_2 = d$ in dimensions above 2. Although we find some discrepancy between our simulations and the values used by Zhang for the exponents $\lambda$ and $\gamma_2$, our simulations seem to be consistent with the scaling expression derived by Zhang for the exponent $\tau$,

$$\tau = 2 + \frac{d-2}{d} \tag{41}$$

**Table III. Simulation Results for Systems (in One, Two, Three, and Four Dimensions) with Open Boundary Conditions Combined with the Conservative Perturbation Mechanism**

| Dimension | $\tau$ | $\gamma_1$ | $1/\gamma_1$ | $\gamma_2$ | $1/\gamma_2$ | $\gamma_3$ | $1/\gamma_3$ | $\gamma_1\gamma_3$ | $1/\gamma_1\gamma_3$ |
|---|---|---|---|---|---|---|---|---|---|
| 1 | 1 | 1 | 1 | 1 | 1 | 1 | 1 | 1 | 1 |
| 2 | 2.21 | 1.45 | 0.66 | 1.97 | 0.50 | 1.34 | 0.75 | 1.94 | 0.50 |
| 3 | 2.47 | 1.64 | 0.60 | 2.65 | 0.37 | 1.61 | 0.62 | 2.64 | 0.37 |
| 4 | 2.61 | 1.68 | 0.58 | 3.09 | 0.32 | 1.85 | 0.54 | 3.11 | 0.31 |

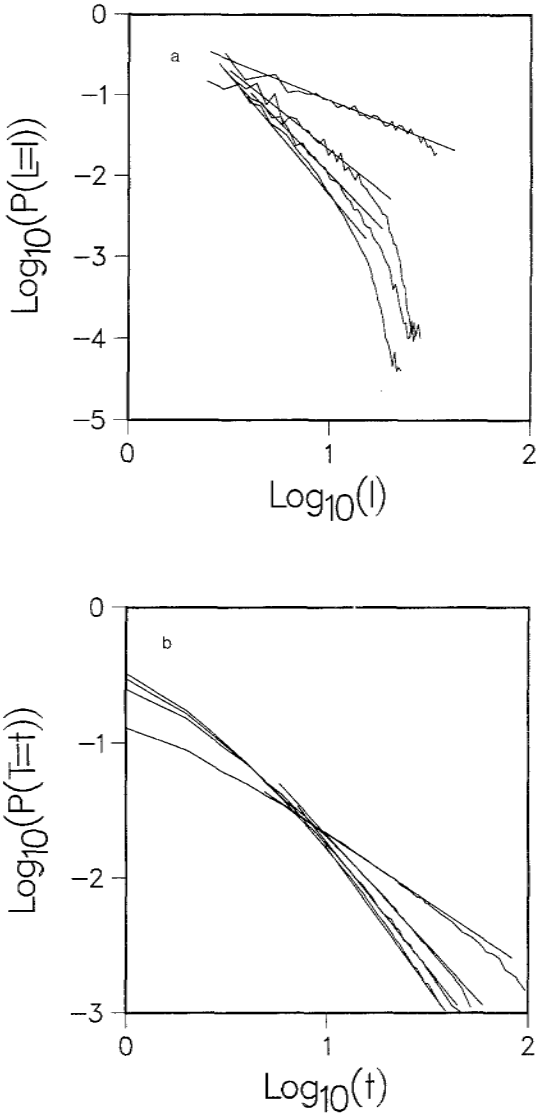


Fig. 10. Simulation results for systems with closed boundary conditions combined with the nonconservative perturbation mechanism. (a) The probability densities for the spatial linear size. (b) The probability densities for the lifetimes. Different curves refer to different spatial dimensions. The slopes of the curves become steeper as the dimension is increased from 2 to 5. See the text for an explanation of the solid straight lines.

A direct comparison with our prediction in Eq. (26) is consistent within the numerical accuracy.

Finally, we wish to comment on a possible critical dimension of the sandpile cellular automaton. It has been suggested that the critical dimension is equal to four.[24,29] We find that the scaling exponents change when going from dimension four to five. This indicates that the critical dimension, if any, is larger than four. However, numerical limitations prevent us from making any definite statement on this point.

## 5.2. Power Spectrum

In order to measure numerically the power spectrum of the stochastic process $J(\tau)$, we make use of Eq. (31). First we generate one realization $j(\tau)$ of duration $T$ containing $R$ avalanches in the following way (see Fig. 6).

### Algorithm 2

1. Set $j(\tau)=0$ for all $\tau$.
2. Perturb the system on a randomly chosen position until an avalanche is activated.
3. Measure the dissipation rate $f_\alpha(\tau)$ of the avalanche.
4. Choose a starting time $\tau_0$ at random and set $j(\tau)=j(\tau)+f_\alpha(\tau-\tau_0)$.
5. Go to 2 until $R$ avalanches have been generated.

Using this procedure, we create a linearly superimposed signal with perturbation rate $v=R/T$. The assumption of no interference between different avalanches was essential for the derivation of Eq. (35). Time sequencies $j(\tau)$ generated according to Algorithm 2 will, of course, fulfil this requirement no matter how high a rate $v$ we choose. If, however, we generate $j(\tau)$ as the directly measured dissipation rate in a finite lattice continuously perturbed with rate $v$, we will have to make $v$ small to be able to neglect interference between simultaneously operating avalanches.

In practice we found in ref. 18 that even for small systems and small finite driving rate $v$ the numerically measured power spectrum of the dissipation signal $j(\tau)$ produced by a continuous perturbation and the one produced using Algorithm 2 could not be distinguished.

Since the resulting representation $j(\tau)$ of the ensemble is a discrete function of time, we use Fourier series. We define the Fourier transform of a signal $j(\tau)$ of duration $T$ as

$$\hat{j}(\omega_k)=\frac{1}{\sqrt{T}}\sum_{\tau=0}^{T-1} j(\tau)e^{-i\omega_k\tau} \tag{42}$$

where the frequency $\omega_k = 2\pi k/T$ for $k = 0, 1, ..., T-1$. The square of the absolute value of Eq. (42) is the corresponding power spectrum of one specific realization of $J(\tau)$. This power spectrum fluctuates strongly. We make an average over many different realizations $j_i(\tau)$ in order to determined the power spectrum $S_J(\omega_k)$ of the stochastic process $J(\tau)$ [cf. Eq. (31)]:

$$S_J(\omega_k) = \frac{1}{M} \sum_{i=1}^{M} |\hat{j}_i(\omega_k)|^2 \tag{43}$$

Generated power spectra are shown in Fig. 11 for a system with closed boundary conditions driven by the nonconservative perturbation mechanism. The forms of spectra for the other versions of the model considered here are identical. We find that all power spectra behave as $1/\omega^2$ irrespective of dimension, choice of perturbation mechanism, and boundary conditions.

The power spectrum obtained by direct numerical measurement should be compared with the measure weighted lifetime distribution function $A$. We focus on systems driven by the nonconservative perturbation mechanism combined with the closed boundary conditions. We can calculate the exponent $\mu$ from Eq. (40) by inserting the measured values for $\tau$ and $\gamma_1$ listed in Table I. We find $\mu = 2.1$, 1.77, 1.69, 1.56 in dimensions 2,

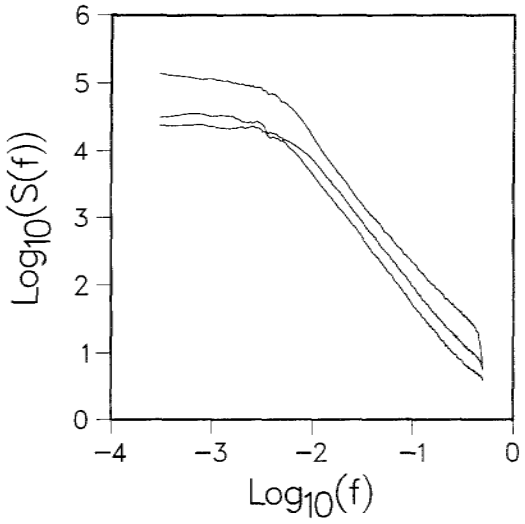


Fig. 11. Power spectra for the total dissipation rate obtained by linear superposition of avalanche signals. The system has closed boundary conditions and is driven by the nonconservative perturbation mechanism. The different curves refer to different dimensions. The dimension decreases from four to two going from bottom to top.

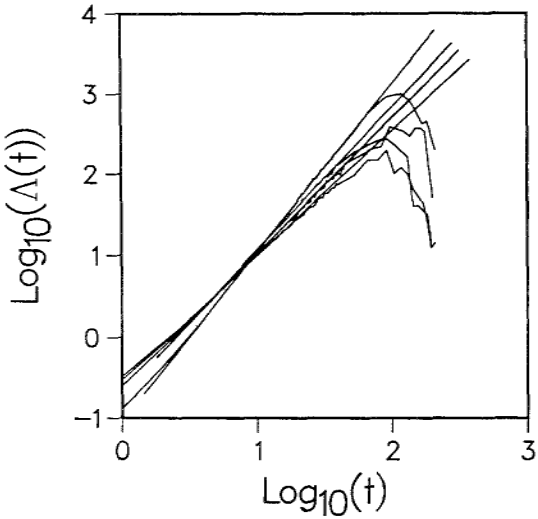


Fig. 12. The weighted lifetime distribution defined in Eq. (36). The results shown are for the closed boundary conditions and the nonconservative perturbation mechanism. The different curves refer to different dimensions. The curves become less steep with increasing dimension. The slopes of the straight lines are calculated from Eq. (40) by use of the measured $\tau$ and $\gamma_1$ listed in Table I.

3, 4, and 5, respectively. As seen in Fig. 12, the $\Lambda(t)$ function appears to satisfy this scaling behavior approximately. The solid lines indicate these slopes. The avalanche signals are assumed to be self-similar in a statistical sense. By inspection of the actual form of the avalanche signals $f_\alpha(\tau)$ this hypothesis appears to be fulfilled (see also ref. 19). Moreover, the $f_\alpha(\tau)$ signals are well approximated by box signals of duration equal to the lifetime $t$ of the avalanche $\alpha$ and height $s/t$, where $s$ is the total dissipation of the avalanche $\alpha$. It follows that the fundamental signal $f_{1,1}(\tau)$ is a s quare box function with $\alpha_\infty = -2$ and from Eq. (39) we conclude that $S_f(\omega) \sim \omega^{-2}$. This conclusion was reached for two-dimensional systems in ref. 18 and also in ref. 19. It is in contradiction to the original claim by Bak *et al.*[3] Although the different sandpile cellular automata exhibit self-organized critical behavior in the sense that distribution functions exhibit power law behavior, the models do not contain the expected $1/f$ power spectrum. However, that self-organized critical models can contain $1/f$ power spectra has recently been demonstrated in a lattice gas model.[17]

## 6. CONCLUSION

We have studied avalanches in different versions of the sandpile cellular automaton. Scaling exponents were measured numerically and

analytically derived scaling relations tested. We found that three properties—the lifetime, the total dissipation, and the spatial linear size—are all connected through scaling relations. The connection between the distribution of weighted lifetimes and the corresponding power spectrum for linearly superimposed avalanches was derived. It was shown that the weighted lifetime distribution must be independent of the avalanche lifetime in order to obtain a $1/f$ power spectrum. Furthermore, we examined the temporal behavior of flow of sand down the slope. The power spectra of the flow were found to behave as $1/f^2$ in all dimensions from 1 to 5.

## APPENDIX A

To calculate the power spectrum of a stochastic process analytically it is most convenient to make use of the autocorrelation function. For a stochastic process which is stationary in the *wide sense* (see below) the power spectrum is determined according to the Wiener–Khinchine theorem as the Fourier transform of the autocorrelation function.

The total dissipation rate $j(\tau)$ at time $\tau$ is given by [see Eq. (27)]

$$j(\tau) = \sum_{\alpha} \sum_{n=-\infty}^{\infty} f_\alpha(\tau - n\delta)\, p^\alpha(n\delta) \tag{A1}$$

As explained in the text following Eq. (28), we introduce an ensemble of stationary systems and turn the total dissipation rate into a stochastic process

$$J(\tau) = \sum_{\alpha} \sum_{n=-\infty}^{\infty} f_\alpha(\tau - n\delta)\, P^\alpha(n\delta) \tag{A2}$$

where $P^\alpha(n\delta)$ denotes the stochastic process associated with the concrete realizations $\alpha, n \mapsto p^\alpha(n\delta)$ belonging to a representation of the ensemble.

In order to determine the power spectrum of the stochastic process, we consider the autocorrelation function

$$\begin{aligned}
\Psi_J(\tau, \tau+\tau_0) &= E[J(\tau)\, J(\tau+\tau_0)] \\
&= \sum_{\alpha}\sum_{\beta}\sum_{n}\sum_{n'} f_\alpha(\tau - n\delta)\, f_\beta(\tau+\tau_0 - n'\delta)\, E[P^\alpha(n\delta)\, P^\beta(n'\delta)] \\
&= \sum_{\alpha}\sum_{n} f_\alpha(\tau - n\delta)\, f_\alpha(\tau+\tau_0 - n\delta)\, E[\{P^\alpha(n\delta)\}^2] \\
&\quad + \sum_{\alpha}\sum_{\beta\neq\alpha}\sum_{n}\sum_{n'\neq n} f_\alpha(\tau - n\delta)\, f_\beta(\tau+\tau_0 - n')\, E[P^\alpha(n\delta)\, P^\beta(n'\delta)]
\end{aligned} \tag{A3}$$

Since with fixed $\alpha$ and $n$ the stochastic variable $P^\alpha(n\delta)$ has the range 0, 1 we have (again with fixed $\alpha$ and $n$) $P^\alpha(n\delta)\,P^\alpha(n\delta) = P^\alpha(n\delta)$. Hence, $E[\{P^\alpha(n\delta)\}^2] = P(\alpha)\,v\delta$, where $v$ is the rate with which avalanches are started. $P(\alpha)$ denotes the probability for an avalanche of type $\alpha$ to occur. Because the avalanches are assumed to be independent we have

$$E[P^\alpha(n\delta)\,P^\beta(n'\delta)] = E[P^\alpha(n\delta)]\,E[P^\beta(n'\delta)] = P(\alpha)\,P(\beta)\,v^2\delta^2 \quad \text{(A4)}$$

By use of these two equations we obtain

$$\Psi_J(\tau, \tau+\tau_0) = v\sum_\alpha P(\alpha)\int_{-\infty}^{\infty} f_\alpha(\tau)\,f_\alpha(\tau+\tau_0)\,d\tau + v^2\sum_\alpha\sum_\beta P(\alpha)\,P(\beta)\int_{-\infty}^{\infty}\int_{-\infty}^{\infty} f_\alpha(\tau)\,f_\beta(\tau')\,d\tau\,d\tau' \quad \text{(A5)}$$

We note that $\Psi_J(\tau, \tau+\tau_0)$ does not depend on $\tau$. Furthermore, the average

$$E[J(\tau)] = v\sum_\alpha \int_0^\infty f_\alpha(\tau)\,P(\alpha)\,d\tau \quad \text{(A6)}$$

is also independent of $\tau$. Such a stochastic process is said to be *stationary in a wide sense.*

Finally, we take the Fourier transform of the autocorrelation function. We observe that the second term in Eq. (A4) is a constant and therefore only contributes to $S_J(\omega = 0)$. Thus we obtain for finite frequencies

$$S_J(\omega) = v\sum_\alpha P(\alpha)\int_{-\infty}^{\infty} f_\alpha(\tau)\int_{-\infty}^{\infty} f_\alpha(\tau+\tau_0)e^{-i\omega\tau_0}\,d\tau_0\,d\tau = v\sum_\alpha P(\alpha)|\hat{f}_\alpha(\omega)|^2 \quad \text{(A7)}$$

## APPENDIX B

In this Appendix we give a detailed discusion of the scaling properties of the power spectrum. The fundamental equation regarding the power spectrum of linearly superimposed signals is

$$S_J(\omega) = v\sum_s\sum_t |\hat{f}_{1,1}(\omega t)|^2 s^2 P(S=s, T=t) \quad \text{(B1)}$$

To investigate the scaling behavior, we have to consider the term

$$|\hat{f}_{1,1}(\omega t)|^2 = \left|\int_{-\infty}^{\infty} f_{1,1}(\tau)e^{-i\omega t\tau}\,d\tau\right|^2 \quad \text{(B2)}$$

more closely. We use Parseval's theorem

$$\frac{1}{2\pi}\int_{-\infty}^{\infty} |\hat{f}_{1,1}(\omega t)|^2 \, d(\omega t) = \int_{-\infty}^{\infty} f_{1,1}^2(\tau) \, d\tau \tag{B3}$$

to obtain limits on the possible scaling behavior of $\hat{f}_{1,1}(\omega t)$. Assume that the time signals have finite energy content, i.e., that the integral on the right-hand side of Eq. (B3) is finite. It follows for the limit of small argument, $\omega t \to 0$, that

$$|\hat{f}_{1,1}(\omega t)|^2 \sim (\omega t)^{\alpha_0} \Rightarrow \alpha_0 > -1 \tag{B4}$$

and for large arguments $\omega t \to \infty$

$$|\hat{f}_{1,1}(\omega t)|^2 \sim (\omega t)^{\alpha_\infty} \Rightarrow \alpha_\infty < -1 \tag{B5}$$

These are the restrictions for the exponents originally obtained by van der Ziel.[49] Using the ideas from Halford,[50] it is possible to make further restrictions on the exponents $\alpha_0$ and $\alpha_\infty$.

Making use of the continuity of the absolute value and Lebesque's convergence theorem, we find

$$\lim_{\omega t \to 0} |\hat{f}_{1,1}(\omega t)|^2 = \left| \int_{-\infty}^{\infty} f_{1,1}(\tau) \, d\tau \right|^2 = 1 \tag{B6}$$

Hence, $\alpha_0 = 0$.

It is not as trivial to put a restriction on the range of $\alpha_\infty$. However, if the time signal $f_{1,1}(\tau)$ is reasonably well-behaved, the corresponding autocorrelation function

$$\Psi_{1,1}(\tau_0) = \lim_{T \to \infty} \frac{1}{2T} \int_{-T}^{T} f_{1,1}(\tau) \, f_{1,1}(\tau + \tau_0) \, d\tau \tag{B7}$$

is everywhere continuous and furthermore the first derivative with respect to $\tau_0$ is without singularities, i.e., everywhere finite. This requirement implies $\alpha_\infty \leqslant -2$. The argument is as follows.

The Wiener–Khinchine theorem expresses the power spectrum as the Fourier transform of the autocorrelation function

$$|\hat{f}_{1,1}(\omega t)|^2 = \int_{-\infty}^{\infty} \Psi_{1,1}(\tau_0) e^{-i\omega t \tau_0} \, d\tau_0 \tag{B8}$$

The inverse Fourier transform leads to

$$\Psi_{1,1}(\tau_0) = \frac{1}{\pi} \int_{0}^{\infty} |\hat{f}_{1,1}(\omega t)|^2 \cos(\omega t \tau_0) \, d(\omega t) \tag{B9}$$

The derivative of the autocorrelation function is given by

$$\frac{d\Psi_{1,1}(\tau_0)}{d\tau_0} = -\frac{1}{\pi}\int_0^\infty |\hat{f}_{1,1}(x)|^2 x \sin(x\tau_0)\, dx \tag{B10}$$

Assuming

$$\begin{aligned} |\hat{f}_{1,1}(x)|^2 &\sim Kx^{\alpha_0} \qquad \text{for} \quad x \leqslant 1 \\ |\hat{f}_{1,1}(x)|^2 &\sim Kx^{\alpha_\infty} \qquad \text{for} \quad x \geqslant 1 \end{aligned} \tag{B11}$$

we obtain for $\tau_0 \leqslant 1$

$$\begin{aligned} \frac{d\Psi_{1,1}(\tau_0)}{d\tau_0} = \frac{-K}{\pi}\Bigg\{ & \int_0^1 x^{\alpha_0+1}\sin(x\tau_0)\, dx \\ & + \int_1^{1/\tau_0} x^{\alpha_\infty+1}\sin(x\tau_0)\, dx + \int_{1/\tau_0}^\infty x^{\alpha_\infty+1}\sin(x\tau_0)\, dx \Bigg\} \end{aligned} \tag{B12}$$

For $\tau_0 \ll 1$ we can use $\sin(x\tau_0) \approx x\tau_0$ in the first two integrals; in the third we substitute $x\tau_0 \mapsto x$ and find

$$\begin{aligned} \frac{d\Psi_{1,1}(\tau_0)}{d\tau_0} = -\frac{K}{\pi}\Bigg\{ & \tau_0\left(\frac{1}{\alpha_0+3} - \frac{1}{\alpha_\infty+3}\right) \\ & + \frac{1}{\tau_0^{\alpha_\infty+2}}\left[\frac{1}{\alpha_\infty+3} + \int_1^\infty x^{\alpha_\infty+1}\sin(x)\, dx\right]\Bigg\} \end{aligned} \tag{B13}$$

from which we obtain that

$$\lim_{\tau_0 \to 0} \frac{d\Psi_{1,1}(\tau_0)}{d\tau_0} < \infty \Rightarrow \alpha_\infty \leqslant -2 \tag{B14}$$

We consider two examples. First assume $f_{s,t}(\tau)$ to be the square box

$$f_{s,t}(\tau) = \begin{cases} s/t & \text{if} \quad 0 < \tau < t \\ 0 & \text{otherwise} \end{cases} \tag{B15}$$

We then have

$$\hat{f}_{s,t}(\omega) = \frac{s}{t}\frac{1 - e^{-i\omega t}}{i\omega} = s\hat{f}_{1,1}(t\omega) \tag{B16}$$

This equation illustrates Eq. (34). Furthermore,

$$|\hat{f}_{1,1}(\omega t)|^2 \sim \begin{cases} 1 & \text{for} \quad \omega t \to 0 \\ (\omega t)^{-2} & \text{for} \quad \omega t \to \infty \end{cases} \tag{B17}$$

Thus, $\alpha_0 = 0$ and $\alpha_\infty = -2$. Second, let $f_{s,t}(\tau)$ be given by

$$f_{s,t}(\tau) = \begin{cases} (4s/t^2)\tau & \text{if } 0 < \tau < t/2 \\ (4s/t^2)(t-\tau) & \text{if } t/2 < \tau < t \end{cases} \tag{B18}$$

We then have

$$\hat{f}_{s,t}(\omega) = \frac{4s}{(t\omega)^2}(2e^{-i\omega t/2} - e^{-i\omega t} - 1) \tag{B19}$$

This equation illustrates Eq. (34). Furthermore,

$$|\hat{f}_{1,1}(\omega t)|^2 \sim \begin{cases} 1 & \text{for } \omega t \to 0 \\ (\omega t)^{-4} & \text{for } \omega t \to \infty \end{cases} \tag{B20}$$

Thus, $\alpha_0 = 0$ and $\alpha_\infty = -4$.

The starting point for the discussion of the scaling behavior of the power spectrum in the intermediate regime $1/t_2 \ll \omega \ll 1/t_1$ corresponding to Eq. (37) is Eq. (38),

$$S_J(\omega) \approx v\omega^{-\mu-1}\left\{\int_{\omega t_1}^{1} t^\mu |\hat{f}_{1,1}(t)|^2\, dt + \int_1^{\omega t_2} t^\mu |\hat{f}_{1,1}(t)|^2\, dt\right\} \tag{B21}$$

Assume again Eq. (B11); then

$$S_J(\omega) = vK\omega^{-\mu-1}\left[\frac{1-(\omega t_1)^{\mu+\alpha_0+1}}{\mu+\alpha_0+1} - \frac{1-(\omega t_2)^{\mu+\alpha_\infty+1}}{\mu+\alpha_\infty+1}\right] \tag{B22}$$

The scaling behavior in the region $\omega t_1 \ll 1$ and $\omega t_2 \gg 1$ is determined by the sign of the exponents $\mu+\alpha_0+1$ and $\mu+\alpha_\infty+1$. We have five different posibilities (see Fig. 13):

1. $\mu+\alpha_0+1<0$ and $\mu+\alpha_\infty+1<0 \Leftrightarrow \alpha_0 < -\mu-1 \Rightarrow S_J(\omega) \sim \omega^{\alpha_0}$.
2. $\mu+\alpha_0+1>0$ and $\mu+\alpha_\infty+1<0 \Leftrightarrow \alpha_\infty < -\mu-1 < \alpha_0$ $\Rightarrow S_J(\omega) \sim \omega^{-\mu-1}$.
3. $\mu+\alpha_0+1>0$ and $\mu+\alpha_\infty+1>0 \Leftrightarrow \alpha_\infty > -\mu-1 \Rightarrow S_J(\omega) \sim \omega^{\alpha_\infty}$.
4. $\mu+\alpha_0+1=0 \Leftrightarrow -\mu-1=\alpha_0 \Rightarrow S_J(\omega) \sim \omega^{\alpha_0}\ln(\omega t_1)$.
5. $\mu+\alpha_\infty+1=0 \Leftrightarrow -\mu-1=\alpha_\infty \Rightarrow S_J S_J(\omega) \sim \omega^{\alpha_\infty}\ln(\omega t_2)$.

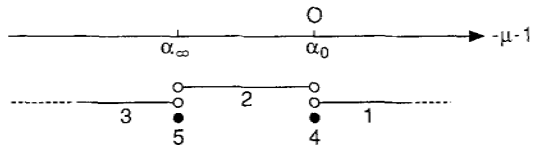


Fig. 13. The five different scaling behaviors of the power spectrum.

## ACKNOWLEDGMENTS

We thank Elisabeth Nicol and especially Mette Jørgensen for advice on the language of this paper. The support and hospitality of NORDITA are gratefully acknowledged. This work was supported by the Danish Natural Science Research Council under grant J.Nr. 11-6836.

## REFERENCES

1. M. B. Weissman, *Rev. Mod. Phys.* **60**:537 (1988).
2. B. Mandelbrot, *The Fractal Geometry of Nature* (Freeman, San Francisco, 1982).
3. P. Bak, C. Tang, and K. Wiesenfeld, *Phys. Rev. Lett.* **59**:381 (1987).
4. P. Alstrøm, P. Trunfio, and H. E. Stanley, in *Random Fluctuations and Pattern Growth: Experiments and Models*, H. H. Stanley and N. Ostrowsky, eds. (Kluwer, Dordrecht, 1989), p. 340.
5. P. Bak, *Physica A* **163**:403 (1990).
6. P. Bak and K. Chen, *Physica D* **38**:5 (1989).
7. P. Bak, K. Chen, and M. Creutz, *Nature* **342**:780 (1989).
8. P. Bak, K. Chen, and C. Tang, *Phys. Rev. Lett. A* **147**:297 (1990).
9. P. Bak and C. Tang, *Physics Today* **42**:S27 (1989).
10. P. Bak, C. Tang, and K. Wiesenfeld, *Phys. Rev. A* **38**:3645 (1989).
11. P. Bak, C. Tang, and K. Wiesenfeld, in *Random Fluctuations and Pattern Growth: Experiments and Models*, H. E. Stanley and N. Ostrowsky, eds. (Kluwer, Dordrecht, 1989), p. 329.
12. J. M. Carlson, J. T. Chayes, E. R. Grannan, and G. H. Swindle, *Phys. Rev. A* **42**:2467 (1990).
13. K. Chen and P. Bak, *Phys. Lett.* **140**:299 (1989).
14. D. Dhar, *Phys. Rev. Lett.* **63**:1659 (1989).
15. D. Dhar and R. Ramaswamy, *Phys. Rev. Lett.* **64**:1613 (1990).
16. G. Grinstein, D.-H. Lee, and S. Sachdev, *Phys. Rev. Lett.* **64**:1927 (1990).
17. H. J. Jensen, *Phys. Rev. Lett.* **64**:3103 (1990).
18. H. J. Jensen, K. Christensen, and H. C. Fogedby, *Phys. Rev. B* **40**:7425 (1989).
19. J. Kertész and L. B. Kiss, *J. Phys. A* **23**:L433 (1990).
20. B. McNamara and K. Wiesenfeld, *Phys. Rev. A* **41**:1867 (1990).
21. S. P. Obukhov, *Phys. Rev. Lett.* **65**:1395 (1990).
22. K. Wiesenfeld, C. Tang, and P. Bak, *J. Stat. Phys.* **54**:1441 (1989).
23. K. Wiesenfeld, J. Theiler, and B. McNamara, *Phys. Rev. Lett.* **65**:949 (1990).
24. P. Alstrøm, *Phys. Rev. A* **38**:4905 (1988).
25. P. Grassberger and S. S. Manna, Some more sandpiles, Physics Department, University of Wuppertal, Preprint, to appear in *J. Phys.* (Paris).
26. T. Hwa and M. Kardar, *Phys. Rev. Lett.* **62**:1813 (1989); *Physica D* **38**:198 (1989).
27. L. P. Kadanoff, S. Nagel, L. Wu, and S. Zhou, *Phys. Rev. A* **39**:6524 (1989).
28. L. P. Kadanoff, *Physica A* **163**:1 (1990).
29. S. P. Obukhov, in *Random Fluctuations and Pattern Growth: Experiments and Models*, H. E. Stanley and N. Ostrowsky, eds. (Kluwer, Dordrecht, 1989), p. 336; see also J. Honkonen, *Phys. Lett. A* **145**:87 (1990).
30. C. Tang, Scalings in avalanches and elsewhere, Institute for Theoretical Physics, University of California, Santa Barbara, preprint, submitted to *Phys. Rev. A*.
31. C. Tang and P. Bak, *Phys. Rev. Lett.* **60**:2347 (1988).

32. C. Tang and P. Bak, *J. Stat. Phys.* **51**:797 (1988).
33. Y.-C. Zhang, *Phys. Rev. Lett.* **63**:470 (1989).
34. P. Bak and C. Tang, *J. Geophys. Res. B* **94**:15635 (1989).
35. P. Bak and K. Chen, Dynamics of earthquakes, in *Fractals and Their Application to Geophysics* (Geological Society of America, Denver, 1990).
36. J. M. Carlson and J. S. Langer, *Phys. Rev. Lett.* **62**:2632 (1989).
37. K. Ito and M. Matsuzaki, *J. Geophys. Res.* **95**:6853 (1990).
38. A. Sonnette and D. Sonnette, *Europhys. Lett.* **9**:192 (1989).
39. H. Takayasu and M. Matsuzaki, *Phys. Lett.* **131**:244 (1988).
40. G. W. Baxter and R. P. Behringer, *Phys. Rev. A* **42**:1017 (1990).
41. W. Clauss, A. Kittel, U. Rau, J. Parisi, J. Peinke, and R. P. Huebener, Self-organized critical behavior in low-temperature impact ionization breakdown of *p*-Ge, Physikalisches Institut, Tübingen, Preprint.
42. P. Evesque and J. Rajchenbach, *Phys. Rev. Lett.* **62**:44 (1989).
43. G. A. Held, D. H. Solina, II, D. T. Keane, W. J. Haag, P. M. Horn, and G. Grinstein, *Phys. Rev. Lett.* **65**:1120 (1990).
44. H. M. Jaeger, Chu-heng Liu, and Sidney R. Nagel, *Phys. Rev. Lett.* **62**:40 (1989).
45. H. M. Jaeger, C.-H. Liu, S. R. Nagel, and T. A. Witten, Friction in granular flow, James Franck Institute, Chicago, Preprint.
46. D. K. C. MacDonald, *Noise and Fluctuations: An Introduction* (Wiley, New York, 1962).
47. P. Z. Peebles, Jr., *Probability, Random Variables, and Random Signal Principles* (McGraw-Hill, 1987).
48. A. Papoulis, *The Fourier Integral and its Applications* (McGraw-Hill, 1962).
49. A. van der Ziel, *Physica* **16**:359 (1950).
50. D. Halford, *Proc. IEEE* **56**:251 (1968).